Journal of Zhejiang University SCIENCE A
ISSN 1009-3095 (Print); ISSN 1862-1775 (Online)
www.zju.edu.cn/jzus; www.springerlink.com
E-mail: jzus@zju.edu.cn

Prediction of wall deposition behaviour in a pilot-scale spray dryer using deposition correlations for pipe flows

KOTA K., LANGRISH T.A.G.†

(*School of Chemical and Biomolecular Engineering, University of Sydney, Sydney, Australia*)

†E-mail: tim.langrish@usyd.edu.au

Received Aug. 10, 2006; revision accepted Oct. 24, 2006

Abstract: The particle deposition behaviour of skim milk, water and maltodextrin in the conical section of a pilot-scale spray dryer was predicted using simple correlations for particle depositions in pipes. The predicted particle deposition fluxes of these materials were then compared with the measured deposition fluxes. The predicted particle deposition regimes of the spray dryer were expected to be in the diffusional and mixed (diffusional and inertial) regimes, but the experimental results suggested that the particle deposition was mainly in the inertial regime. Therefore, using the pipe correlations for predicting deposition in a pilot-scale spray dryer suggests that they do not sufficiently represent the actual deposition behaviour. This outcome indicates that a further study of particle flow patterns needs to be carried out using numerical simulations (computational fluid dynamics, CFD) in view of the additional geometrical complexity of the spray dryer.

Key words: Spray dryer, Pipe correlations, Particle deposition
doi:10.1631/jzus.2007.A0301 **Document code:** A **CLC number:** TQ018; TE624.41

INTRODUCTION

Abbott (1990) reported that wall deposition in spray dryers may pose a potential fire risk and compromise hygiene requirements, and reduce product quality and yield. Spray dryer hazards include ignition of explosible dust clouds, dust deposits, bulk powder deposits and flammable vapour. Kieviet (1997) noted that wall deposition affected the residence time distribution of particles, and particularly that an important factor in determining residence times with high wall deposition rates was the time taken by particles to slide down the conical wall of a spray dryer. Sticking of particles to the walls and to each other, and sliding of wall deposits, are therefore important issues. A combination of modified near-wall airflow patterns and inlet temperature distribution was suggested by Chen *et al.*(1993) to significantly reduce wall deposition in industrial-scale spray drying of milk, with such changes being cheaper than making major modifications in the design of an existing dryer.

A key issue in wall deposition in spray dryers is the collisions of particles or droplets with walls, the fate of the particles after the collisions, which is linked with the issue of stickiness. Glass transitions occur in foodstuffs containing sugars and acids, between a glassy and a more sticky (rubbery) state above a certain temperature (Bhandari *et al*., 1997). The glass transition temperature (T_g) is defined as a temperature at which a material-specific change in physical state from rubbery to a glassy mechanical solid state or glassy to a rubbery state. The glass transition temperature is a property of an amorphous material. There are methods for detecting this transition (Adhikari *et al*., 2001), including mechanical devices, such as a stirred laboratory-scale apparatus using a propeller to turn a powder sample with controlled temperature and moisture content. This method was found by Papadakis and Bahu (1992) to give reproducible results. The glass transition temperature may be important both for cohesion of particles to one another (the situation that was strictly involved in this test) and adhesion of particles to

walls. A Differential Scanning Calorimeter may also be used to measure the glass transition by detecting the change in specific heat capacity associated with the transition temperature from a glassy to the rubbery phase. Stickiness can begin 10~20 K above the glass transition temperature (Bhandari *et al*., 1997), since the critical viscosity associated with stickiness does not necessarily occur exactly at the phase transition point. Bhandari *et al*.(1997) gave formulae to predict the glass transition temperature for sugars and acids as a function of the moisture content. For skim milk powder, Ozmen and Langrish (2002) also noted good agreement between glass transition and sticky-point temperatures (with a slight offset).

In this work, the gas to wall deposition process from the viewpoint of the collision process is studied. The flux of particles colliding with the wall of dyers is a function of the fluid flow patterns in the dryers, and computational fluid dynamics (CFD) can provide guidance in this area, as suggested by Masters (1996). The particle trajectories can be predicted using CFD, enabling the prediction of whether or not the particles hit the walls and the temperatures and moisture contents of such particles. The behaviour of the particle stickiness as a function of temperature and moisture content, both at the surface and within the particles, determines whether the particles bounce off the walls, adhere to them, or cohere to other particles that are already adhering to the walls, but this study has primarily focused on the collision processes at the walls.

THEORY

Considerations in using CFD for predicting the deposition behaviour of particles in spray dryers

There is a general problem in using a conventional k-ε turbulence model to predict particle deposition in fully-developed turbulent pipe flows, particularly for small particles. In this approach, each of the root mean square (RMS) values of the fluctuating components of velocity (in each direction) is assumed to be equal and related to the turbulence kinetic energy as described by Eq.(1):

$$u'_{\mathrm{RMS}} = v'_{\mathrm{RMS}} = w'_{\mathrm{RMS}} = \sqrt{2k/3}. \tag{1}$$

However, the actual RMS value of the fluctuating component of radial velocity near the wall is substantially smaller near the wall, than the isotropic decomposition of the turbulence kinetic energy given in Eq.(1). To overcome this problem, Uijttewaal and Oliemans (1996) and Wang *et al*.(1997) used large eddy simulations (LES) and direct numerical simulations (DNS) to solve the Navier-Stokes equations, with one-way coupling for the particle motion in simple geometries such as pipe and channels respectively. They obtained good agreement with the dataset of McCoy and Hanratty (1977), but the high cost of the computation limits this approach. Uijttewaal and Oliemans (1996) used the Reynolds numbers up to 42000 for LES and 5000 for DNS simulations with 130000 particles of different sizes. Wang *et al*.(1997) performed LES for Reynolds numbers up to 79400 with 20000 particles. Recent studies (Wu and Durbin, 2001; Rodi, 2006) indicate that Reynolds numbers of up to 148000 in a turbine cascade channel could be achieved for DNS simulations, but at considerable computational cost. In LES simulations, Rodi (2006) simulated a Reynolds number of 2800000 for a simple geometry such as Ahmed car body, again at high computational cost.

The RANS (Reynolds Averaged Navier Stokes) approach, as implemented in most commercial CFD codes using turbulence models such as k-ε and Reynolds stress models, such as CFX, FLUENT and KIVA, is cost effective. However, the accurate prediction of wall deposition of particles depends on having sufficient resolution of the near-wall turbulent behaviour of the flow, with current RANS approaches not having this capability. Matida *et al*.(2000) suggested that optimizing the parameters in the RANS equations to give accurate near-wall statistics on the primary flow may improve this situation for wall deposition without significantly affecting the prediction of bulk flow.

Shuen *et al*.(1983) found that such approaches overestimate deposition velocities significantly for small particles ($\tau^+<10$), while underestimating them for larger particles. The dimensionless particle relaxation time is defined as $\tau^+=(1/18)(\rho_\mathrm{p}/\rho_\mathrm{f})(d_\mathrm{p}u^*/\nu)^2$, where ρ_p is the particle density, ρ_f is the fluid (gas) density, u^* is the friction velocity, d_p is the particle diameter, and ν is the kinematic viscosity of the gas. According to (Matida *et al*., 2000), particle release conditions affect deposition velocities of these small

particles (τ^+<10) while having no significant influence on the deposition velocity of larger particles (τ^+>20). Matida *et al*.(2000) did simulations of the deposition process and considered that the pipe deposition data of Liu and Agarwal (1974) and McCoy and Hanratty (1977) were good enough to compare with the results of such simulations. The agreement was generally good, with a slight decrease in dimensionless deposition velocity being noted for τ^+>100 in both their simulations and the data of McCoy and Hanratty (1977). There was little influence of the particle density for τ^+>20 for particles having dimensionless particle relaxation times (τ^+) of 3.2 and 27.9. Marchioli *et al*.(2003) found that diffusional deposition was dominant in their direct numerical simulations of wall deposition, whereas free flight, or direct impact, deposition was dominant for particles having dimensionless particle relaxation times (τ^+) of 111.6. The free flight mechanism could be reproduced by a ballistic deposition equation, with the bulk conditions being the initial conditions.

Despite the weaknesses of the RANS approach, Yilmaz and Cliffe (2000) used it, with Eulerian gas-phase modelling and Lagrangian particle tracking within the CFD code FLUENT, allowing for drag, thermophoresis, buoyancy and gravity. They used this approach for modelling fly ash deposition from a high-temperature flue gas to a superheater tube and compared the predictions from the simulation with experimental deposition data from a small-scale furnace using an air-cooled probe. They found that the effects of thermophoresis were not very significant, even though the temperature gradient was large, at 400 K/mm, because small particles of 6~8 μm could not reach the 9 mm thick thermal boundary layer, which was much smaller than the 49.5 mm thick hydrodynamic boundary layer. The degree of agreement between simulation and experiment was dependent on the particle size, with the best agreement being achieved for 16~26 μm diameter particles. Despite the limitations in the RANS approach, the agreement was good for these particle sizes, with the discrepancies being less than 10%.

The question is whether or not information about the deposition of particles from pipe flows may be of assistance in predicting the wall deposition behaviour in spray dryers.

Deposition of particles in pipes

In flowing systems, each particle has to penetrate the boundary layer before reaching the wall. Papavergos and Hedley (1984) suggested a diagram of the dimensionless deposition velocity as a function of the dimensionless particle relaxation time. The data sources and the data themselves are largely the same as those in (McCoy and Hanratty, 1977). The data are still current, as shown by the recent study of Matida *et al*.(2000), who did DNS of the particle deposition process in pipes and considered that the deposition data of Liu and Agarwal (1974) and McCoy and Hanratty (1977) were good enough to compare with the results of such simulations. In addition, these data were used by Shams *et al*.(2001), again suggesting that the dataset remains valid despite the length of time since its publication. Masuda and Matsusaka (1997) also used these data, pointing out that there is a large scatter in the data, possibly due to the effects of different bulk (pipe) Reynolds numbers and ratios of particle to fluid density.

The experimental data show a large scatter as non-sticky materials were used in most of them, so measurements must be performed to evaluate the applicability of this information from spray dryers.

The actual deposition velocity is the particle flux to the wall [kg/(m^2·s)] divided by the constant bulk particle concentration far from the wall (kg/m^3). The dimensionless deposition velocity (v_d^+) is the actual deposition velocity divided by the friction velocity (u^*) defined as $u^*=\sqrt{\tau_w/\rho_f}$, where τ_w is the wall shear stress. The gas density and kinematic velocities are standard physical properties. The particle diameters may be measured, and the wall shear stress can be estimated by various methods depending on the geometry and the flow conditions.

From (Masuda and Matsusaka, 1997):

$$u^*=\bar{u}\sqrt{f/2}. \tag{2}$$

The average fluid velocity is $\bar{u}$, and f is the friction factor, which is given by:

$$f=0.0791Re^{-1/4},\ \text{for}\ 3\times10^3<Re<10^5. \tag{3}$$

Hence:

$$u^*=0.2\,\bar{u}\,Re^{-1/8}. \tag{4}$$

In the sub-micron range, τ^+ is typically less than 0.15, and particles follow the fluid motion. In this range, Brownian motion is the main wall deposition mechanism. At higher dimensionless particle relaxation times, the dimensionless deposition velocities are given by the following relationships (Masuda and Matsusaka, 1997):

$$\begin{aligned} v_d^+ &= 0.065\,Sc^{-2/3}, && \text{for } \tau^+ < 0.2; \\ v_d^+ &= 3.5\times10^{-4}(\tau^+)^2, && \text{for } 0.2 < \tau^+ < 20; \\ v_d^+ &= 0.18, && \text{for } \tau^+ > 20. \end{aligned} \quad (5)$$

where Sc is the Schmidt number, which is the kinematic viscosity of the gas (ν) divided by the Brownian diffusivity of particles (D) given by the equation:

$$D = \frac{kTC_c}{3\pi\mu d_p}. \quad (6)$$

where μ is the dynamic viscosity of the gas, k is Boltzmann's constant, which is 1.38×10^{-23} J/K, T is the absolute temperature, and C_c is Cunningham's slip correction factor, normally close to unity. In the present work, this theory will be compared with experimental data for wall deposition in spray dryers.

DESCRIPTION OF EXPERIMENTAL EQUIPMENT

In this study, a pilot-scale spray dryer (cylinder on cone) (Fig.1) with diameter of 0.8 m and height of 1.5 m was used. The conical section of the spray dryer was equipped with three stainless steel plates (75 mm×75 mm) at three locations connected with tubes to external containers for collecting the liquid. The dryer was then sealed to prevent any air entering and leaving the dryer except through the air inlet and outlet, respectively. The three locations were the top, middle and bottom plate positions of the conical section, with their distances from the top of the conical section being 0.158, 0.315, 0.473 m, respectively, as shown in Fig.2.

The atomizer used was an ultrasonic two-fluid type; model number MAD 0331 B1 BD, from PNR Ltd (Bromsgrove, UK). The atomizer uses external mixing, where the air and liquid streams leave the nozzle independently and are combined and mixed outside the nozzle, so that the air and liquid flow rates can be controlled independently. The spray produced was a poly-disperse full-cone spray with an angle of 17°~20°. A typical particle size distribution from this atomizer for water ranged from 5.8~129 μm, with a Sauter mean of 10 μm. A laser diffraction device was used for particle size measurement (Malvern Particle Size Analyzer 2600C) with a size range of 5.8 μm to 564 μm. In this experiment, the liquid was fed to the system by a six-rotor peristaltic pump (ISMATEC model mp-ge).

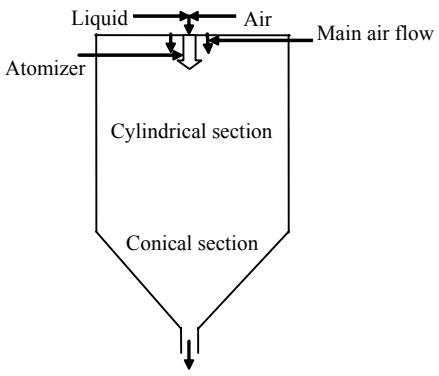

Fig.1 Pilot-scale spray dryer showing the cylindrical and conical sections

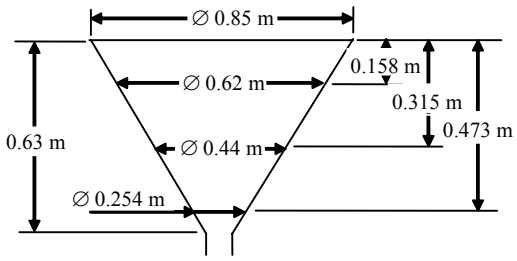

Fig.2 Conical section of the spray dryer showing the distances of three positions where the deposition fluxes were measured and the wall shear stresses were estimated

EXPERIMENTAL METHOD

The spray dryer was initially started by introducing air without any heating at a flow rate of about 150 kg/h and then allowed to reach a steady-state condition over a period of 10~15 min. Cold air was used to minimize the extent of evaporation, which would otherwise complicate the analysis of the wall

deposition behaviour due to its effect on the droplet sizes. The swirl vane angle was 0°, following the work of Ozmen and Langrish (2005), which showed that this angle gives the minimum amount of wall deposition in this dryer design. The water was sprayed at three different flow rates (27 ml/min, 13.6 ml/min, 6.5 ml/min). For each of the three flow rates, the ratio of liquid to air flow rates was maintained at a nearly constant value by changing the air flow rate through the atomizer (by changing the atomizer air flow rates from 26 L/min to 20 L/min and 10 L/min) so that the particle size distribution was similar. At each of the flow rates, the spray dryer was run for a known period so that sufficient (measurable) deposition was obtained on the plates. The duration (30 min~2 h) of spraying was recorded. At the end of the experiment, for small amounts of deposition, the plates were removed carefully and weighed to estimate the total deposition. For larger amounts of deposition, the weight of water collected in the flasks at the bottom of tubes connected to each of the plates was measured. Since the area of the plates was known, the deposition fluxes were also estimated.

CALCULATION PROCEDURE

The procedure used to predict the deposition fluxes is based on the use of flux correlations for the deposition of dry particles in pipes and will now be described in more detail with sample calculations.

The walls of the spray dryer, including the cone, were treated as if they were the walls of a pipe for the estimation of the wall shear stress (τ_w). In order to estimate the shear stress (τ_w), the needed friction factor ($f/2=\varphi$) is related to the dimensionless group $\tau_w/(\rho U^2)$ as follows (Coulson and Richardson, 1997):

$$\tau_w/(\rho U^2)=\varphi=f/2. \quad (7)$$

The friction factor term ($f/2=\varphi$) is in turn related to the Reynolds number as shown in Eq.(8), so that:

$$\tau_w=0.0396Re^{-1/4}(\rho U^2). \quad (8)$$

Eq.(8) gives the wall shear stress (τ_w) in terms of the Reynolds number and the average fluid velocity, which are all known, since the density (ρ=1.2 kg/m^3) and the viscosity of air [1.8×10^{-5} kg/(m·s)] are known. The average velocity of air through the spray dryer can be estimated by dividing the measured mass flow rate (150 kg/h, Kota and Langrish, 2006) by the known cross-sectional area of the spray dryer and the air density. The wall shear stress for the conical section of the spray dryer can be estimated at each of the three locations where the plates are placed to measure the deposition rates.

For the top section, the distance of the plate from the top of the 0.31 m radius conical section is 0.158 m. The volumetric flow rate Q is calculated by dividing the mass flow rate by the density of air ρ_f =1.2 kg/m^3.

Q=150/1.2=125 m^3/h=0.035 m^3/s,
$U=Q/A=4Q/(\pi D^2)=0.035/(\pi\times0.31^2)=0.116$ m/s,
$Re=DU\rho/\mu=2\times0.31\times0.116\times1.2/(1.8\times10^{-5})$
=4794 (turbulent),
$\tau_w=0.039\times4794^{-0.25}(1.2\times0.116^2)=7.568\times10^{-5}$ Pa,

where U is velocity of the air.

Similarly, the shear stresses at the middle and bottom locations are calculated to be 2.822×10^{-4} Pa and 2.149×10^{-3} Pa, respectively. The friction velocities are calculated from the wall shear stresses obtained for the top, middle and bottom sections, showing that the wall shear stress increases towards the bottom of the conical section. The friction velocity of the top section ($\tau_w=7.568\times10^{-5}$ Pa) is calculated as follows:

$$u^*=\sqrt{\tau_w/\rho_f}=\sqrt{7.568\times10^{-5}/1.2}=7.941\times10^{-3} \text{ m/s}.$$

Similarly, the friction velocities of the middle and bottom sections are estimated to be 0.0153 m/s and 0.0423 m/s, respectively. If the wall friction velocities are different, then the particle deposition velocities will be different, which leads to different dimensionless particle relaxation times even if the particle sizes are the same at each of the plate locations. This logic suggests that the deposition fluxes of particles on each of the plates in the conical section should be different. The estimation of the dimensionless particle relaxation times (Table 1) helps in identifying the main mechanism of deposition on the walls. The deposition regimes include the diffu-

sional, mixed (diffusion and inertial) and inertial ones. Fig.3 gives a typical droplet size distribution for a water flow rate of 27 ml/min and an air flow through the ultrasonic atomizer of 26 L/min.

Table 1 The estimated dimensionless particle relaxation time (τ^+) for the top, middle and bottom sections at d_p 10%, 50% and 90% respectively

Cut diameter (μm)	Dimensionless particle relaxation time τ^+		
	Top section	Middle section	Bottom section
$d_{p10\%}$=5.8	4.278×10^{-4}	1.588×10^{-3}	1.214×10^{-2}
$d_{p50\%}$=18.9	4.542×10^{-3}	1.686×10^{-2}	1.289×10^{-2}
$d_{p90\%}$=45.8	2.667×10^{-2}	9.902×10^{-2}	7.568×10^{-1}

The wall shear stress τ_w at the top, middle and bottom sections is 7.568×10^{-5} Pa, 2.822×10^{-4} Pa, 2.149×10^{-3} Pa, respectively

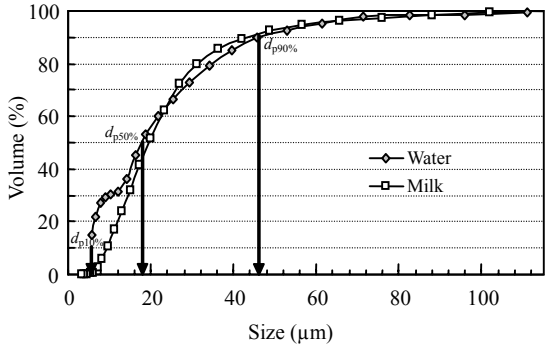

Fig.3 Droplet size distribution showing the cut diameters at 10%, 50% and 90% for water and milk flow rates of 27 ml/min through the ultrasonic atomizer

The $d_{p10\%}$ is the mid point that covers the volume percent of droplets in the range from 0~20%, similarly $d_{p50\%}$ covers the range 20%~80% and $d_{p90\%}$ covers the range 80%~100%. This is because the volume percentage is equal to the mass percentage, since the density is constant, and these size ranges represent a mass balance that accounts for all the droplets in the particle size distribution. These cut diameters are used here, since the particle size distributions are known in the spray dryer, from which it is possible to estimate the dimensionless particle relaxation times at different plate locations for each of the average (cut) diameters independently.

The dimensionless particle relaxation times are calculated as $\tau^+=(\rho_p/18\rho_f)(d_p u^*/\nu)^2$, kinematic viscosity of gas $\nu=\mu/\rho=1.8\times10^{-5}/1.2=1.5\times10^{-5}$ m^2/s, where density of particle ρ_p=980 kg/m^3 (water droplets). For example, at the top of the dryer, where $u^*=7.941\times10^{-3}$ m/s, and for the average size at $d_{p10\%}$ of 5.8 μm (obtained from Fig.4), the dimensionless particle relaxation time is:

$$\tau^+=\left(\frac{980}{18\times1.2}\right)\left(\frac{5.8\times10^{-6}\times7.941\times10^{-3}}{1.5\times10^{-5}}\right)^2=4.278\times10^{-4}.$$

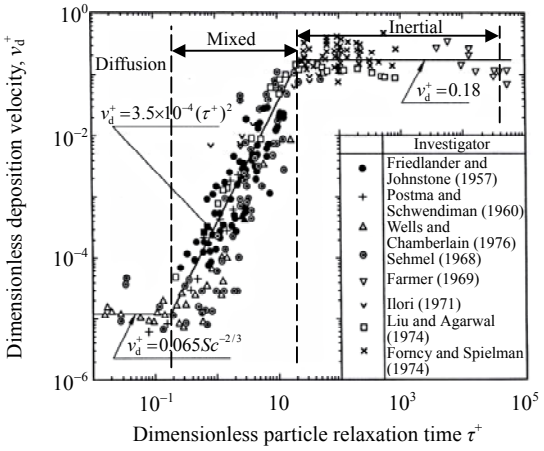

Fig.4 Experimental deposition data in vertical flow systems (after Papavergos and Hedley, 1984)

Similarly, for $d_{p50\%}$ (20%~80%, 6.7~34.1 μm)= 18.9 μm, $\tau^+=4.542\times10^{-3}$ and $d_{p90\%}$ (80%~100%, 34.1~111 μm)=45.8 μm, $\tau^+=2.667\times10^{-2}$. The results for other cases are shown in Table 1 for dimensionless relaxation times and in Table 2 for the dimensionless deposition velocities.

Table 2 The estimated dimensionless deposition velocities (v_d^+) for the top, middle and bottom sections at d_p 10%, 50% and 90%, obtained from (Papavergos and Hedley, 1984), corresponding to the dimensionless particle relaxation times (τ^+) in Table 1

Cut diameter (μm)	Dimensionless deposition velocity v_d^+		
	Top section	Middle section	Bottom section
$d_{p10\%}$=5.8	1.000×10^{-5}	1.000×10^{-5}	1.000×10^{-5}
$d_{p50\%}$=18.9	1.000×10^{-5}	1.000×10^{-5}	1.000×10^{-5}
$d_{p90\%}$=45.8	1.000×10^{-5}	1.000×10^{-5}	2.005×10^{-4}

The wall shear stress τ_w at the top, middle and bottom sections is 7.568×10^{-5} Pa, 2.822×10^{-4} Pa, 2.149×10^{-3} Pa, respectively

The dimensionless particle relaxation times yield estimates of the dimensionless particle deposition velocities for flow in a pipe (Papervegos and

Hedley, 1984). The dimensionless particle deposition velocities estimated in this way were used for the prediction of the deposition fluxes in the conical section of the spray dryer. The actual velocity of particles towards the wall was then estimated for each of the sections of the spray dryer by multiplying the dimensionless particle velocity by the friction velocity. Table 3 shows the results for each section.

Table 3 Actual deposition velocities of particles for the top, middle and bottom sections of the spray dryer

Cut diameter (μm)	Deposition velocity v_d (m/s)		
	Top section	Middle section	Bottom section
$d_{p10\%}$=5.8	7.941×10^{-8}	1.530×10^{-7}	4.230×10^{-7}
$d_{p50\%}$=18.9	7.941×10^{-8}	1.530×10^{-7}	4.230×10^{-7}
$d_{p90\%}$=45.8	7.941×10^{-8}	1.530×10^{-7}	8.480×10^{-6}

The friction velocity u^* at the top, middle and bottom sections is 7.941×10^{-3} m/s, 0.0153 m/s, 0.0423 m/s, respectively

The average concentration of droplets at cut diameters of 10%, 50% and 90% for water may be calculated from the measured particle size distributions ranging between 5.8~111 μm (Fig.3), as follows.

For $d_{p10\%}$=5.8 μm, the concentration is calculated by estimating the amount in this size class (0~6.7 μm, 0~20%). A typical calculation for this case is as follows:

$$V_d=\pi(d_p)^3/6=\pi(5.8\times10^{-6})^3/6=1.022\times10^{-16}\ \text{m}^3,$$

$$N_d/T=\frac{Q_w}{V_d}=\frac{4.5\times10^{-7}}{1.022\times10^{-16}}=4.405\times10^{9}\ \text{s}^{-1},$$

$$\rho_{tot}=\frac{N_d/T}{Q_a}=\frac{4.405\times10^{9}}{0.035}=1.259\times10^{11}\ \text{particles/m}^3,$$

$M_d=V_d\times\rho_d=1.022\times10^{-16}\times980=1.001\times10^{-13}$ kg,

$\rho_{ad}=\rho_{tot}\times V_p/100=1.259\times10^{10}\times6.65/100$
$=8.369\times10^{9}$ particles/m^3,

$C_{pm}=\rho_{ad}\times M_p=8.369\times10^{9}\times1.001\times10^{-13}$
$=8.379\times10^{-4}$ kg/m^3,

$C_{ap10\%}=\sum$(particle concentrations between 0 and 20%, 0~6.7 μm)
$=1.562\times10^{-3}$ kg/m^3,

where V_d is the volume of droplet (m^3), N_d is the number of droplets, T is time, Q_w is volumetric flowrate of water (m^3/s), ρ_{tot} is total number density, Q_a is volumetric flowrate of air through the dryer, M_d is droplet mass, ρ_d is the droplet density, ρ_{ad} is actual droplet density, V_p is volume percent from particle size distribution, C_{pm} is particle mass concentration, M_p is particle mass, $C_{ap10\%}$ is average mass concentration at $d_{p10\%}$.

Similarly average mass concentration of droplets for each size class,

$d_{p50\%}$ (18.9 μm)
$=7.251\times10^{-3}$ kg/m^3 (size range 7.8~34.1 μm),

$d_{p90\%}$ (45.8 μm)
$=1.903\times10^{-3}$ kg/m^3 (size range 39.5~111 μm),

The total particle concentration for water
$=\sum$(particle concentrations between 0 and 100%)
$=1.072\times10^{-2}$ kg/m^3.

The particle concentrations for skim milk at 8.8% and 30% solids by weight and maltodextrin (8.8% solids by weight) that are used here were obtained from the particle size distributions in (Kota and Langrish, 2006; Langrish *et al*., 2007). The total particle concentration for skim milk (30%, 0.51 kg/h) was estimated to be 4.046×10^{-3} kg/m^3. Similarly, the total concentrations for skim milk (8.8%) and maltodextrin (8.8%) were estimated by assuming that the particle size distributions are similar for both cases because they have the same solids concentration. The total particle concentration for skim milk (8.8%, 0.03 kg/h, Kota and Langrish, 2006) was estimated to be 2.38×10^{-4} kg/m^3.

The individual concentrations at particular cut diameters were estimated in a similar way as discussed in the previous sections to calculate the deposition velocities for the top, middle and bottom sections for skim milk and maltodextrin as well as for water.

RESULTS AND DISCUSSION

Table 4 shows the water deposition fluxes determined by the method already described, which is based on deposition data for pipe flows. The experimental concentration of particles is estimated from the mass concentration of all the particles ranging between 5.8~111 μm, which is the average concentration of particles in the dryer. Then the experimental deposition velocity is calculated by dividing the

experimental flux by this average concentration. This concentration is assumed to be constant throughout the spray dryer i.e. at top, middle and bottom positions of the conical section.

This is equivalent to assuming that the dryer is well mixed in terms of both particles and gas.

This approach was used by Ozmen and Langrish (2003) for assessing relative changes in dryer performance, so this approach appears to be useful.

Table 5 shows the experimental and predicted deposition fluxes for water with different flow rates at the top, middle and bottom locations of the pilot-scale spray dryer, predicted using the pipe deposition approach. Table 5 also shows the data on the deposition fluxes when spray drying skim milk and maltodextrin at different solids concentrations and flow rates from the literature, for the same dryer.

Table 4 Predicted deposition fluxes for different particle sizes of water at the top, middle and bottom sections of the dryer and the total fluxes at each position

Concentration (kg/m^3)	f_d [kg/(m^2·s)]		
	Top section	Middle section	Bottom section
2.684×10^{-3} ($d_{p10\%}$=8.65 μm)	2.131×10^{-10}	4.106×10^{-10}	1.135×10^{-9}
7.736×10^{-3} ($d_{p50\%}$=32.73 μm)	6.143×10^{-10}	1.184×10^{-9}	1.711×10^{-8}
2.961×10^{-4} ($d_{p90\%}$=90.25 μm)	2.351×10^{-11}	2.344×10^{-10}	3.786×10^{-8}
Total flux	8.510×10^{-10}	1.829×10^{-9}	5.610×10^{-8}

The deposition flux $f_d=C/v_d$, where C is concentration; the friction velocity u^* at the top, middle and bottom sections is 7.941×10^{-3} m/s, 0.0153 m/s, 0.0423 m/s, respectively

Factors that may be used to compare the data are the solids flow rate and the main air flow rate into the dryer. The solids flow rate into the dryer is an important factor, since the particle concentration or the number density can influence the collision of particles on the walls of the dryer. At higher concentrations (number densities), the deposition fluxes are expected to be higher due to the correspondingly larger numbers of particles colliding with the walls of the dryer. The main air flow rate into the dryer is also expected to have a significant effect on the deposition fluxes because the particles are affected by the flow patterns inside the dryer. At higher air flow rates, it is possible that the deposition velocities will be higher because the higher air flow rates increase the friction velocities at the walls. This situation will increase the dimensionless particle relaxation times and dimensionless particle deposition velocities, resulting in higher collision rates with the walls, increasing the deposition flux. However, a high flow rate of air also means that the particle concentration decreases, thus possibly decreasing the deposition fluxes, so the effect of increasing air flow rates may either increase or decrease the deposition

Table 5 Experimental and predicted fluxes for different materials in the top, middle and bottom locations of this pilot-scale dryer

Materials	Plate locations	Q_a (kg/h)	Q_l (kg/h)	Q_s (kg/h)	F_{ae} [kg/(m^2·s)]	f_p [kg/(m^2·s)]	C_{abp} (kg/m^3)
Skim milk (8.8%) (Kota and Langrish, 2006)	Top	150	0.31	0.03	3.00×10^{-7}	3.089×10^{-10}	2.289×10^{-4}
	Middle				4.56×10^{-7}	5.952×10^{-10}	
	Bottom				6.86×10^{-7}	5.529×10^{-9}	
Skim milk (30%) (Kota and Langrish, 2006)	Top	150	1.70	0.51	2.06×10^{-5}	3.089×10^{-10}	3.891×10^{-3}
	Middle				2.92×10^{-5}	5.952×10^{-10}	
	Bottom				5.69×10^{-5}	5.529×10^{-9}	
Skim milk (8.8%) (Ozmen and Langrish, 2002)	Top	60	1.80	0.17	3.61×10^{-6}	1.545×10^{-10}	1.297×10^{-3}
	Middle				3.61×10^{-6}	2.976×10^{-10}	
	Bottom				3.61×10^{-6}	8.229×10^{-10}	
Skim milk (8.8%) (Langrish *et al*., 2005)	Top	68	1.50	0.15	4.17×10^{-6}	1.545×10^{-10}	1.259×10^{-3}
	Middle				8.06×10^{-6}	2.976×10^{-10}	
	Bottom				1.17×10^{-5}	8.229×10^{-10}	
Maltodextrin (8.8%) (Langrish *et al*., 2005)	Top	68	1.50	0.15	1.86×10^{-6}	1.545×10^{-10}	1.259×10^{-3}
	Middle				2.78×10^{-6}	2.976×10^{-10}	
	Bottom				4.17×10^{-6}	8.229×10^{-10}	
Water	Top	113	1.62	−	8.29×10^{-5}	8.510×10^{-10}	1.072×10^{-2}
	Middle				4.47×10^{-4}	1.829×10^{-9}	
	Bottom				8.89×10^{-4}	5.610×10^{-8}	

Q_a is air flow rate through the dryer, Q_l is liquid flow rate, O_s is solids flow rate, F_{ae} is average experimental flux, f_p is predicted flux, C_{abp} is average bulk particle concentration

fluxes. The deposition fluxes are discussed in the following section for the main air flow rates of 150 kg/h and 70 kg/h.

(1) 150 kg/h (First two rows of Table 5)

From Table 5, it can be seen that, for the case with a air flow rate of 150 kg/h, at high solids flow rates (0.51 kg/h) the plates have high fluxes compared with the case of low solids flow rates (0.03 kg/h) into the dryer. The measured deposition fluxes on the plates are two orders of magnitude higher at the higher solids flow rate (0.51 kg/h) compared with the lower solids flow rate (0.03 kg/h). The higher concentration of particles is also likely to result in particle/droplets coalescing to form agglomerates, which can also increase the deposition on the walls due to greater particle size. However, the particle concentrations in these cases are very dilute, so agglomeration is unlikely to occur. These observations are consistent with the reasoning that higher solids concentrations are likely to lead to higher wall collision rates and hence deposition fluxes.

(2) 70 kg/h (3~5 rows of Table 5)

In other studies with an air flow rate of 60~68 kg/h, the solids flow rate into the dryer was constant at 0.15 kg/h. In this case, the experimental fluxes for skim milk and maltodextrin indicate that they have similar trends, with lower deposition fluxes at the top plate compared with the middle and bottom plates. It can be seen that, for the same solids concentration, there was a significant difference in fluxes between skim milk and maltodextrin. The deposition fluxes are higher for the skim milk compared with those of maltodextrin, which could be due to the presence of a fat layer (Kim *et al*., 2002; Buma, 1971; Rennie *et al*., 1999) on skim milk particles making these particles stickier than the maltodextrin particles (Langrsih *et al*., 2005). These comparisons show the effects of material properties on deposition fluxes.

From Table 5, no conditions were covered where the solids flow rate was the same, while the air flow rate was different. In addition, the differences in the estimated average bulk particle concentrations in Table 5 were calculated from the combined solids and air flow rates, so they account for the combined effects of changing these variables. An assessment of the combined effects of changing these variables can be obtained by dividing the average experimental fluxes by the average bulk particle concentrations, both in Table 5, which give estimates of the actual deposition velocities shown in Table 6.

Most of the actual deposition velocities given in Table 6 are of the order of millimeters per second, but the range is still wide, from 1.31 mm/s for 8.8% skim milk (Kota and Langrish, 2006) to 83 mm/s for water. Given that the particle size distributions and operating conditions for the dryer were still within the same order of magnitude, yet the actual deposi-

Table 6 The experimental deposition velocities (v_d) estimated from the average experimental fluxes divided by the average bulk concentrations

Materials	Plate locations	Q_a (kg/h)	Q_l (kg/h)	Q_s (kg/h)	v_d (mm/s)
Skim milk (8.8%) (Kota and Langrish, 2006)	Top	150	0.31	0.03	1.31
	Middle				1.99
	Bottom				2.99
Skim milk (30%) (Kota and Langrish, 2006)	Top	150	1.70	0.51	5.29
	Middle				7.50
	Bottom				14.60
Skim milk (8.8%) (Ozmen and Langrish, 2002)	Top	60	1.80	0.17	2.78
	Middle				2.78
	Bottom				2.78
Skim milk (8.8%) (Langrish *et al*., 2005)	Top	68	1.50	0.15	3.31
	Middle				6.40
	Bottom				9.29
Maltodextrin (8.8%) (Langrish *et al*., 2005)	Top	68	1.50	0.15	1.48
	Middle				2.21
	Bottom				3.31
Water	Top	113	1.62	−	7.73
	Middle				41.70
	Bottom				82.90

Q_a is air flow rate through the dryer, Q_l is liquid flow rate, O_s is solids flow rate, v_d is average deposition velocity

tion velocities vary by almost two orders of magnitude (1.31~83 mm/s). This situation further highlights the significant differences between the deposition behaviours for different materials and of dry and wet deposition.

Predicted and experimental fluxes

The predicted fluxes are at least an order of magnitude lower than the experimentally measured fluxes (Table 5), indicating that the application of pipe deposition calculations underpredicts the deposition in the spray dryer, which is a more complex geometry than a pipe. Not only is the geometry more complex, but the physical processes are more complex. In pipe flow, there is usually no nozzle directing the particles towards the walls, but the nozzle-induced and nozzle-directed flow is significant in a spray dryer. However, it is worthwhile to note that the trends for the predicted fluxes agree with the trends seen experimentally, in terms of having lower deposition on the top plate compared with the middle and bottom plates.

The predicted deposition fluxes were compared with the experimental fluxes in terms of equivalent dimensionless particle deposition velocities at various locations in the spray dryer, depending on the regimes of particle deposition as seen in Fig.4. The dimensionless particle deposition times and velocities were plotted in Fig.5 for water, milk and maltodextrin to compare the experimental and the predicted deposition fluxes. The experimental deposition velocities were estimated by the methods described in previous sections, assuming that the particles are uniformly distributed inside the dryer. Then the experimental dimensionless relaxation times for water (and other materials) were obtained from the empirical correlations depending on the location of the particle regimes in Fig.4, corresponding to each experimental dimensionless deposition velocity.

In order to have a uniform comparison method between predicted and experimental fluxes for skim milk, maltodextrin and water, a typical estimation procedure for water to estimate the experimental dimensionless deposition velocities and times is shown in Table 7.

Fig.5 shows that the experimental results of the dimensionless particle deposition velocities for water, milk and maltodextrin are much higher than the predicted values, because the predicted values are based on experimental data for dry particle deposition. From the estimates based on particle size, friction velocities, dimensionless velocities and particle relaxation times, it can be seen that the particles are expected to deposit in the diffusional and mixed regimes. However, the actual dimensionless deposition velocities show that they deposit, effectively, in the

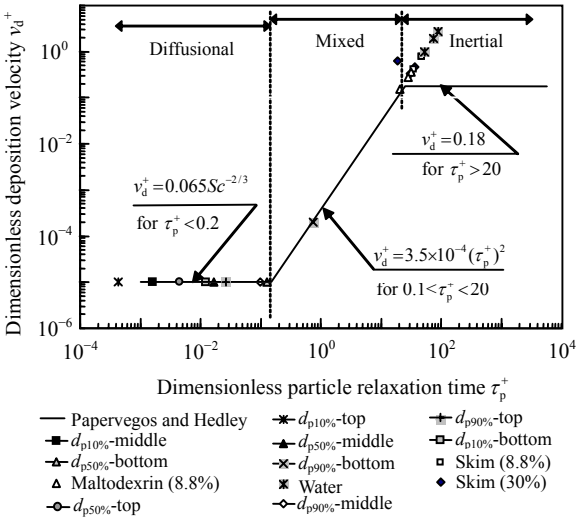

Fig.5 Predicted dimensionless particle deposition velocities and times for water, skim milk (30% and 9%, solids w/w) and maltodextrin (9%, solids w/w). The predicted values of v_d^+ and τ^+ were estimated at the top, middle and bottom positions of the conical section of the spray dryer for each of the cut diameters at 10% ($d_{p10\%}$), 50% ($d_{p50\%}$) and 90% ($d_{p90\%}$)

Table 7 Experimental and predicted fluxes and corresponding deposition velocities of water for the top, middle and bottom sections of the spray dryer

Location	f_e [kg/(m^2·s)]	f_p [kg/(m^2·s)]	Experimental v_d (m/s)	Experimental v_d^+ (v_d/u^*)	Experimental τ^+
Top section	8.290×10^{-5}	8.510×10^{-10}	7.730×10^{-3}	0.974	52.748
Middle section	4.470×10^{-4}	1.829×10^{-9}	4.170×10^{-2}	2.725	88.242
Bottom section	8.890×10^{-4}	5.610×10^{-8}	8.290×10^{-2}	1.960	74.843

f_e is experimental flux, f_p is predicted flux; the friction velocity u^* at the top, middle and bottom sections is 7.941×10^{-3} m/s, 0.0153 m/s, 0.0423 m/s, respectively

inertial regime. The experimental results in Fig.5 correspond to the particles being sticky and/or wet. This situation suggests that dry particle depositions do not sufficiently represent the deposition behavior of wet particles. It also suggests that the simplified picture of gas flow patterns results in under-estimation of the actual deposition fluxes. Therefore, CFD simulations such as using RANS for the flow patterns may be helpful in resolving the more complex gas and particle flow patterns inside the spray dryer and their effects on the deposition fluxes.

CONCLUSION

Simple correlations for particle deposition for pipes were used to predict the deposition in the conical section of a pilot-scale spray dryer for water, skim milk and maltodextrin. The correlations suggested that the predicted particle deposition for the spray dryer would be expected to be in the diffusional and mixed (diffusional and inertial) regimes, but the actual experimental results showed the particle deposition to be mostly in the inertial regime. Therefore, the pipe correlations do not sufficiently represent the actual deposition behaviour, which indicates that a much more detailed study of particle flow patterns needs to be carried out using CFD.

References

Abbott, J.A., 1990. Prevention of Fires and Explosions in Dryers—A User Guide, 2nd Ed. Institution of Chemical Engineers, Rugby.

Adhikari, B., Howes, T., Bhandari, B.R., Truong, V., 2001. Stickiness in foods: A review of mechanisms and test methods. *International Journal of Food Properties*, **4**(1):1-33. [doi:10.1081/JFP-100002186]

Bhandari, B.R., Datta, N., Howes, T., 1997. Problems associated with spray drying of sugar-rich foods. *Drying Technology*, **15**(2):671-684.

Buma, T.J., 1971. Free fat in spray-dried whole milk. 5. Cohesion; Determination, influence of particle size, moisture content and free-fat content. *Netherlands Milk and Dairy Journal*, **25**(2):107-122.

Chen, X.D., Lake, R., Jebson, S., 1993. Study of milk powder deposition on a large industrial dryer. *Trans. I. Chem. E.*, **71**(C3):180-186.

Coulson, J.M., Richardson, J.F, 1997. Chemical Engineering, Volume 1, 5th Edition. Pergamon Press, Oxford.

Farmer, R.A., 1969. ScD Thesis, MIT, USA.

Forney, L.J., Spielman, L.A., 1974. Deposition of coarse aerosols from turbulent flow. *Journal of Aerosol Science*, **5**(3):257-271. [doi:10.1016/0021-8502(74)90061-5]

Friedlander, S.K., Johnstone, H.F., 1957. Deposition of suspended particles from turbulent gas streams. *Industrial and Engineering Chemistry*, **49**(7):1151-1156. [doi:10.1021/ie50571a039]

Ilori, T.A., 1971. Turbulent Deposition of Particles Inside Pipes. Ph.D Thesis, University of Minnesota, USA.

Kieviet, F.G., 1997. Modelling Quality in Spray Drying. Ph.D Thesis, T.U. Eindhoven, The Netherlands, p.72.

Kim, E.H.J., Chen, X.D., Pearce, D., 2002, Surface characterization of four industrial spray-dried dairy powders in relation to chemical composition, structure and wetting property. *Colloids and Surfaces B: Biointerfaces*, **26**(3):197-212. [doi:10.1016/S0927-7765(01)00334-4]

Kota, K., Langrish, T.A.G., 2006. Fluxes and patterns of wall deposits for skim milk in a pilot-scale spray dryer. *Drying Technology*, **24**(8):993-1001. [doi:10.1080/07373930600776167]

Langrish, T.A.G., Chan, W.C., Kota, K., 2007. Comparison of maltodextrin and skim milk wall deposition rates in a pilot-scale spray dryer. *Powder Technology* (in Press).

Liu, B.Y.H., Agrawal, J.K., 1974. Experimental observation of aerosol deposition in turbulent flow. *Journal of Aerosol Science*, **5**(2):145-155. [doi:10.1016/0021-8502(74)90046-9]

Marchioli, C., Giusti, A., Salvetti, M.V., Soldati, A., 2003. Direct numerical simulation of particle wall transfer and deposition in upward turbulent pipe flow. *International Journal of Multiphase Flow*, **29**(6):1017-1038. [doi:10.1016/S0301-9322(03)00036-3]

Masters, K., 1996. Deposit-Free Spray Drying: Dream or Reality? Proceedings of the 10th International Drying Symposium (IDS '96), Drying '96, Krakow, Poland, **A**:52-60.

Masuda, H., Matsusaka, S., 1997. Particle Deposition and Re-entrainment. *In*: Gotoh, K., Masuda, H., Higashitani, K. (Eds.), Powder Technology Handbook, 2nd Ed. Marcel Dekker, New York, P.143-154.

Matida, E.A., Nishino, K., Tori, K., 2000. Statistical simulation of particle deposition on the wall from turbulent dispersed pipe flow. *International Journal of Heat and Fluid Flow*, **21**(4):389-402. [doi:10.1016/S0142-727X(00)00004-7]

McCoy, D.D., Hanratty, T.J., 1977. Rate of deposition of droplets in annular two-phase flow. *International Journal of Multiphase Flow*, **3**(4):319-331. [doi:10.1016/0301-9322(77)90012-X]

Ozmen, L., Langrish, T.A.G., 2002. Comparison of glass transition temperature and stick-point temperature for skim milk powder. *Drying Technology*, **20**(6):1177-1192. [doi:10.1081/DRT-120004046]

Ozmen, L., Langrish, T.A.G., 2003. A study of the limitations to spray dryer outlet performance. *Drying Technology*, **21**(5):895-917. [doi:10.1081/DRT-120021691]

Ozmen, L., Langrish, T.A.G., 2005. Experimental investiga-

tion into wall deposition of milk powder in spray dryers. *Developments in Chemical Engineering and Mineral Processing*, **13**(1-2):91-108.

Papadakis, S.E., Bahu, R.E., 1992. The sticky issues of drying. *Drying Technology*, **10**(4):817-837.

Papavergos, P.G., Hedley, A.B., 1984. Particle deposition behaviour from turbulent flows. *Trans. I. Chem. E. (Chem. Eng. Res. Design)*, **62**(5):275-295.

Postma, A.K., Schwendiman, L.C., 1960. Studies in Micrometrics: I. Particle. Deposition in Conduits as a Source of Error in Aerosol Sampling. Hanford Lab Report HW 65308, Richland, Washington, USA.

Rennie, R.P., Chen, X.D., Hargreaves, C., Mackereth, A.R., 1999. A study of the cohesion of dairy powders. *Journal of Food Engineering*, **39**(3):277-284. [doi:10.1016/S0260-8774(98)00158-7]

Rodi, W., 2006. DNS and LES of some engineering flows. *Fluid Dynamics Research*, **38**(2-3):145-173. [doi:10.1016/j.fluiddyn.2004.11.003]

Sehmel, G.A., 1968. Aerosol Deposition from Turbulent Airstreams in Vertical Conduits. Report BNWL-578, Battelle Memorial Institute, Richland, Washington, USA.

Shams, M., Ahmadi, G., Rahimzadeh, H., 2001. Transport and deposition of flexible fibers in turbulent duct flows. *Journal of Aerosol Science*, **32**(4):525-547. [doi:10.1016/S0021-8502(00)00099-9]

Shuen, J.S., Chen, L.D., Faeth, G.M., 1983. Evaluation of a stochastic model of particle dispersion in a turbulent round jet. *AIChE Journal*, **29**(1):167-170. [doi:10.1002/aic.690290127]

Uijttewaal, W.S.J., Oliemans, R.V.A., 1996. Particle dispersion and deposition in direct numerical and large eddy simulations of vertical flows. *Physics of Fluids*, **8**(10):2590-2604. [doi:10.1063/1.869046]

Wang, Q., Squires, K.D., Chen, M., McLaughlin, J.B., 1997. On the role of the lift force in turbulence simulations of particle deposition. *International Journal of Multiphase Flow*, **23**(4):749-763. [doi:10.1016/S0301-9322(97)00014-1]

Wells, A.C., Chamberlain, A.C., 1969. Deposition of dust from turbulent gas streams. *Atmospheric Environment*, **3**(4):494-496. [doi:10.1016/0004-6981(69)90081-X]

Wu, X., Durbin, P.A., 2001. Evidence of longitudinal vortices evolved from distorted wakes in a turbine passage. *Journal of Fluid Mechanics*, **446**:199-228.

Yilmaz, S., Cliffe, K.R., 2000. Particle deposition simulation using the CFD code FLUENT. *Journal of the Institute of Energy*, **73**(494):65-68.